Comput Geosci (2014) 18:851–867
DOI 10.1007/s10596-014-9430-2

ORIGINAL PAPER

Parallel simulation of groundwater non-point source pollution using algebraic multigrid preconditioners

George Kourakos · Thomas Harter

Received: 18 October 2013 / Accepted: 9 June 2014 / Published online: 1 July 2014
© Springer International Publishing Switzerland 2014

Abstract The simulation of non-point source pollution in agricultural basins is a computationally demanding process due to the large number of individual sources and potential pollution receptors (e.g., drinking water wells). In this study, we present an efficient computational framework for parallel simulation of diffuse pollution in such groundwater basins. To derive a highly detailed velocity field, we employed algebraic multigrid (AMG) preconditioners to solve the groundwater flow equation. We compare two variants of AMG implementations, the multilevel preconditioning provided by Trilinos and the BoomerAMG provided by HYPRE. We also perform a sensitivity analysis on the configuration of AMG methods to evaluate the application of these libraries to groundwater flow problems. For the transport simulation of diffuse contamination, we use the streamline approach, which decomposes the 3D transport problem into a large number of 1D problems that can be executed in parallel. The proposed framework is applied to a 2,600-km^2 groundwater basin in California discretized into a grid with over 11 million degrees of freedom. Using a Monte Carlo approach with 200 nitrate loading realizations at the aquifer surface, we perform a stochastic analysis to quantify nitrate breakthrough prediction uncertainty at over 1,500 wells due to random, temporally distributed nitrate loading. The results show that there is a significant time lag between loading and aquifer response at production wells. Generally, typical production wells respond after 5–50 years depending on well depth and screen length, while the prediction uncertainty for nitrate in individual wells is very large—approximately twice the drinking water limit for nitrate.

G. Kourakos (✉) · T. Harter
University of California, Davis, CA, USA
e-mail: giorgk@gmail.com

Keywords Non point source pollution · Algebraic multigrid · Diffuse pollution · Parallel computing · Contaminant transport · Streamline simulation

1 Introduction

Groundwater is a major resource of drinking water, particularly in semiarid areas associated with agricultural activities. Yet, in such areas, due to intensive use of industrial and animal fertilizers, groundwater has been susceptible to spatially and temporally continuous pollution for nearly half a century [37]. Most agricultural contamination falls into the category of non-point source (NPS) or diffuse pollution. Numerous studies [18, 26, 43, 46, 47, 54, 60, 65, 72, 76] and reports [37, 75, 78] highlight the worldwide extent of the problem and stress the imperative need for more enhanced management practices [20, 41, 57].

Sustainable management of agricultural diffuse pollution is a vital issue, and the development of suitable tools to evaluate the impact of proposed management scenarios remains an active arena for research [11]. In addition, it is very important to further our understanding regarding the transport and fate of pollutants, the range of travel times, and the impact of uncertainty, and identify links between sources and receptors [54], where receptors here include wells, springs, and streams receiving groundwater.

For several decades, groundwater flow and transport models have been invaluable tools for understanding flow and transport mechanisms and also for supporting decision making processes. However, methods to assess NPS pollution of groundwater are quite limited and can generally be grouped into three categories [62]: index, statistical, and physically based methods. For example, DRASTIC [2] is a widely used index-based tool that aggregates

information such as soil type, topography, recharge, etc. using expert-assigned indexing levels and returns a composite vulnerability assessment map. Similarly, statistical methods such as multivariate statistics [48], regression analysis [64], artificial neural networks [3, 50, 82] etc. are employed to extract relationships between control variables (potential sources, environmental conditions) and water quality data in receptors to provide a tool to assess potential groundwater quality impacts.

Physically based methods explicitly capture the flow and transport dynamics that govern the contamination processes. These methods are based on the solution of partial differential equations of groundwater flow and contaminant transport. Physical or process-based approaches provide better insights into flow and transport dynamics than indexing or statistical methods and allow for a wide range of analyses and assessments, including sensitivity, scenario, and stochastic analyses. A major drawback of physically based models is that their implementation is computationally demanding. NPS pollution often takes place in large agricultural basins that extend several hundreds or thousands of square kilometers, while individual sources such as crop fields, dairy lagoons/corrals, septic systems, etc. vary in extent from less than a few hectares to few hundreds of hectares. Groundwater and pollutant discharge to streams or to a large array of irrigation wells (in semiarid and arid basins) forces highly localized flow and transport systems. Therefore, the simulation of very large agricultural basins with sufficiently detailed discretization to account for the proper transport dynamics between the large assembly of relatively small but heterogeneous sources and the affected array of spatially distributed groundwater discharge locations (receptors) would potentially require systems with many millions of degrees of freedom. The large contrast between the extent of groundwater basins and the size and number of contributing sources and affected receptors makes the simulation of NPS pollution a challenging problem, despite current software and hardware developments.

Researchers have utilized process-based models to simulate diffuse pollution mostly in relatively small catchments [28, 56, 59, 80]. Bonton et al. [13] used the numerical model HydroGeoSphere to simulate nitrate transport within a well capture zone using a model with 92,000 degrees of freedom (dof), while [29] discretized a small catchment of 0.12 km^2 into about 28,000 grid cells and simulated the fate of nitrate using MODFLOW, MODPATH, and MT3D. In many studies, researchers simulate the diffuse pollution in large-scale basins at the expense of model resolution, using coarse discretization. Refsgaarda et al. [69] simulated two large groundwater basins in Denmark using 1–5-km resolution grid, while [53] simulated NPS contamination in a 95,560-km^2 agricultural basin using multiscale grid cells that vary between 1 and 8 km^2. Flipo et al. [27] simulated the fate of nitrate in a 1,200-km^2 groundwater basin using a discretization of 8,513 elements (e.g., each element covered 0.14 km^2 approximately). Jiang and Somers [46] combined MODFLOW and MT3D to model a 112-km^2 basin using approximately 15,000 dofs. Almasri and Kaluarachchi [4] and [23] simulated a 388 and 550-km^2 catchments, respectively, using a single layer in the vertical discretization.

In process-based methods, the major computational limitation of fully 3D approaches stems from the simulation of transport. To alleviate this, researchers have adopted the streamline approach, which simplifies a fully 3D transport problem into multiple 1D transport problems that are trivial to solve [7, 19, 24, 33, 39, 45, 66]. The streamline approach has found broad applicability in petroleum engineering [8, 10, 12, 17]. The majority of studies that have adopted this approach to NPS pollution have employed variants of particle-tracking methods to calculate resident time distributions and well capture zone delineation [58, 71, 74, 79]

Recently, [51] and [52] developed a NPS assessment tool (NPSAT) that employs the streamline transport approach on a highly resolved steady-state groundwater flow field to derive an ensemble of unit response functions (URF) for each discharge point of interest (e.g., wells, streams etc.,). The URFs are stored in a GIS database and can be used for predictions by convolution with actual spatiotemporally distributed pollutant loading functions to rapidly calculate breakthrough curves (BTCs). The approach has two distinct advantages. First, based on the premise of steady-state flow (see [51] for full justification of the assumptions), the transport problem can be separated from the flow problem and second, using the URF concept, the transport problem becomes independent of the loading history. However, the NPSAT requires a highly detailed resolution around the receptors to avoid the weak sink problem [73] during backward particle tracking. In addition, the scale of the discretization at the aquifer surface needs to be on the same order as the scale of the individual contributing recharge and pollution sources. Therefore, the simulation of large agricultural groundwater basins leads to a very large system of linear equations.

Typically, large systems are solved using Krylov subspace methods (e.g., preconditioned conjugate gradient (PCG), generalized minimal residual method (GMRES), ORTHOMIN, BiCGSTAB, etc), yet the convergence of these methods tends to slow down considerably as the systems become larger [70]. Moreover, as systems become larger, the increased time of each operation (e.g., matrix vector multiplication per iteration) results in severe loss of efficiency. To alleviate the shortcomings of the Krylov subspace methods, many researchers use multigrid methods for which, in theory, the convergence rates are independent of the mesh size.

The multigrid methods are divided into two categories, geometric and algebraic multigrid methods. Geometric multigrid methods are suitable for systems discretized into regular grids, while algebraic multigrid (AMG) methods are suitable for irregularly discretized systems. AMG methods are algorithmically more complex methods compared to Krylov subspace methods. Libraries are now available that can be used as an interface to AMG methods, but these are not frequently used in groundwater flow simulations [6, 9, 55, 61] due to the fact that the typical groundwater flow simulation packages such as MODFLOW, IWFM, Sutra, HydroGeoSphere do not provide an interface to multigrid solvers [36].

In this paper, we demonstrate the use of the AMG method in a modified parallel version of the NPSAT toolbox [52] to derive a highly detailed, steady-state groundwater flow field for a simulation domain with millions of dofs. We employed two C++ libraries, Trilinos [40] and HYPRE [25], which implement variants of AMG methods, to perform a sensitivity analyses over the configuration parameters of the AMG solvers and provide guidelines for similar problems.

The highly resolved groundwater velocity field is subsequently used in a streamline transport model to simulate the fate of nitrate in large groundwater basins. The method is applied to investigate 200 years of nitrate transport from a 2,600-km^2 source area to 1,500 individual large production wells and 65-km gaining streams in the Modesto subbasin of the Central Valley aquifer, California.

The next section provides a brief description of the governing equations and outlines the fundamental parts of the simulated approach. The third and fourth sections outline the algebraic multigrid methods and the parallelization of the NPSAT toolbox. We then apply the proposed methods to a large-scale simulation of nitrate transport in the Modesto aquifer, California, to quantify uncertainty about pollutant transport time and concentration variability among wells and streams.

2 Overview of the non-point source modeling framework

2.1 Construction phase

The NPS assessment tool is based on three critical assumptions: (1) groundwater flow is steady state, (2) transverse dispersion is negligible, and (3) reactions may include first-order degradation/decay and instantaneous adsorption [51]. The NPSAT consists of two phases, the construction phase and the implementation phase. During the construction phase, groundwater flow is simulated with sufficiently detailed discretization around wells, streams, or other sources or receptors of interest. Due to the highly non-uniform distribution of boundary stresses, we apply the finite element method (FEM), which allows for locally variable size discretization. The groundwater flow field provides the basis for the streamline transport simulation. Note that this method was specifically developed for diffuse pollution problems where all or most recharge sources are associated with an identifiable and relevant level of pollutant concentration and where a large number of discrete receptors or compliance discharge surfaces (CDS) exist (e.g., wells, stream reaches).

To identify the pathways of contaminants that are associated with each particular CDS, a large number of particles are released in the immediate vicinity of the CDS. The particles are tracked backwards until they exit the aquifer, thus defining streamlines. Streamlines consist of a set of positional vectors $X=\{\mathbf{x}_0,\mathbf{x}_1,\ldots,\mathbf{x}_{n,}\}$ that hold the coordinates of the streamline and a set of velocity norms $V=\{v_0,v_1,\ldots,v_n\}$, which contain the velocities at the points of the positional vectors. Note that we are using backward particle tracking that associates each streamline with a contamination source, thus identifying contributing land uses within the source area of a CDS.

For each streamline, we solve the 1D transport problem:

$$
\begin{aligned}
R\frac{\partial c}{\partial t} &= \frac{\partial}{\partial x}\left(D\frac{\partial x}{\partial x} - vc\right) - \lambda Rc \\
&\text{subject to:} \\
c(x)_{t=0} &= 0\,\forall x \in [0,\, L] \\
c(\mathbf{x}_n)_{t>0} &= 1 \\
\left(\frac{\partial c}{\partial t}\right)_{x=\mathbf{x}_o} &= 0
\end{aligned}
\tag{1}
$$

where $c\,(x,t)$ is the solute concentration at point x and time t, v is the pore velocity, D is the dispersion coefficient, λ is the first-order degradation (or decay) constant, and R is the retardation factor. Dispersion $D=\tilde{\alpha}_L v$ is a function of the effective macrodispersivity, $\tilde{\alpha}_L$. The latter, $\tilde{\alpha}_L=f\,(L)$, is typically scaled relative to the length of the streamline L [31, 34]. In the formulation of the transport problem (1), we do not require any knowledge of loading. Instead, a continuous unit loading is applied at the source side $\mathbf{x}_n$. Solving the transport problem (1) we calculate the unit response function (URF) at the CDS side $\mathbf{x}_0$ by shifting the solution to (1) by the basic time unit defining the temporal discretization of the NPS loading function (e.g., 1 year for annually varying loading) and subtracting it, for a given time, from the original solution. The URFs are subsequently archived into a geodatabase and can be used during the implementation phase. In addition to URFs, archives are also established for the coordinates of point $\mathbf{x}_{n,}$ and the velocity v_0 (see below).

2.2 Implementation phase

In the implementation phase, actual BTCs for each CDS are computed as a response to actual pollutant loading functions. The typical form of a loading function is a time series of spatially variable loading rates, varying, e.g., by field, possibly grouped into land-use or crop type categories. Therefore, the first step during the implementation phase is to associate the points $\mathbf{x}_n$ with the associated field or land-use types that have a known loading function. Next, the loading functions are convolved with the URFs to derive the streamline BTCs. The convolution operator is a fast operator that involves only analytical calculations and the execution time is practically negligible. Let $f_L(t)$ be a loading function, which is associated with the URF $g_i^j(t)$ where the indices i and j correspond to the ID of the streamline and the ID of the CDS, respectively. The discrete form of convolution operator is expressed as follows:

$$G_i^j(t) = f_L * g_i^j = \sum_{\zeta=0}^{t} f_L(t-\zeta)\, g_i^j(\zeta) \tag{2}$$

Where $G_i^j(t)$ is the actual BTC in response to the loading function $f_L(t)$ for the streamline i, ζ is a free variable that increases in the summation at time step intervals, and t is the total simulation time.

Finally, the actual BTC for the j CDS $\bar{G}^j(t)$ is the weighted average of the individual streamline BTCs $G_i^j(t)$, e.g., $\bar{G}^j(t) = \sum_{i=1}^{Ns} v_0^i \cdot G_i^j(t) \Big/ \sum_{i=1}^{Ns} v_0^i$, where the weights are taken equal to the amount of flow that each streamline contributes to the CDS.

Most of the NPSAT processes can be executed with current commodity personal computers. But the first step of the construction phase, the computation of the steady-state flow field, can be highly demanding in terms of memory and CPU requirements. In the next section, we outline the basics of the algebraic multigrid method, which is used to alleviate this shortcoming.

3 Algebraic multigrid methods

Multigrid methods are becoming standard parallel processing tools for solving linear system of equations arising from discretization of partial differential equations and are considered among the fastest solvers available [1]. Multigrid methods are based on the observation that the error of a linear system can be split into rough and smooth error components. Iterative methods, such as Krylov subspace methods, can effectively reduce rough errors on the fine grid while the smooth errors can be eliminated on coarser grids. Therefore, the fundamental idea of multigrid methods is to solve the linear system on a hierarchy of grids. Details regarding the rationale of the algorithm can be found in many textbooks [15, 16, 70]. Here, an outline of the basic algebraic multigrid cycle is provided.

First, the simulation domain is discretized and the solution of the partial differential equation is reduced to a system of linear equations of the form $A^0x^0=b^0$. In the case of steady groundwater flow, the matrix A corresponds to the conductance terms, the vector x corresponds to unknown hydraulic head, and the vector b represents the sources/receptors and boundary conditions. The superscript is used here to denote that the system corresponds to the fine discretization level.

AMG methods involve a setup phase, where the grids are constructed along with operators that transfer information between the grids. The construction of grid hierarchy is a recursive process, starting from the finest level. The coarser grid is constructed by aggregating nodes of the finer level. In addition, during the setup phase, the interpolation I_n^{n+1} and restriction I_{n+1}^n operators are computed for each level such that $A^n = I_{n+1}^n A^{n+1} I_n^{n+1}$ and $I_n^{n+1} = {I_{n+1}^n}^T$. These operators are used to transfer information between grids.

After completing the setup phase, the algorithm starts by performing a user-defined number of iterations ("sweeps" in AMG terminology) of an iterative solution method on the finest level $A^0x^0=b^0$. The values of the starting vector are defined by the user. In multigrid terminology, this is variably known as either smoothing or relaxation. Next, the residual is computed and restricted (transferred) onto the next coarser level $r^1 = I_0^1\left(b^0 - A^0x^0\right)$. A smoothing step is again performed on this coarser grid for the system $A^1c^1=r^1$, using zero starting values $c^1 = 0$. A new residual is computed on the current level and restricted onto the next level $r^2 = I_1^2\left(r^1 - A^1c^1\right)$. This process of smoothing and restricting residuals continues until the coarsest level is reached where a direct solve is performed, $c^c = A^{c-1}r^c$, instead of smoothing. The calculated vector c^c is interpolated into the next finer level using the interpolation operator and used to correct the residuals at the current level $c^n = c^n + I_c^n c^c$. The system $A^n c^n = r^n$ is smoothed one more time on this level using the corrected vector c^n as starting values. The smoothed residual is then interpolated into the next finer level and used for correction and smoothing. The process is repeated until the finest level is reached. A graphical illustration of the process is given in Fig. 1. The above algorithm is known as V-cycle. However, there are other options available such as W-cycle and F-cycle [16].

While multigrid (MG) methods can be used as solvers, they can also be used as efficient preconditioners for Krylov subspace methods: After the setup phase in the MG method, an iterative solver is chosen to solve the system, such as PCG or GMRES, and the MG method

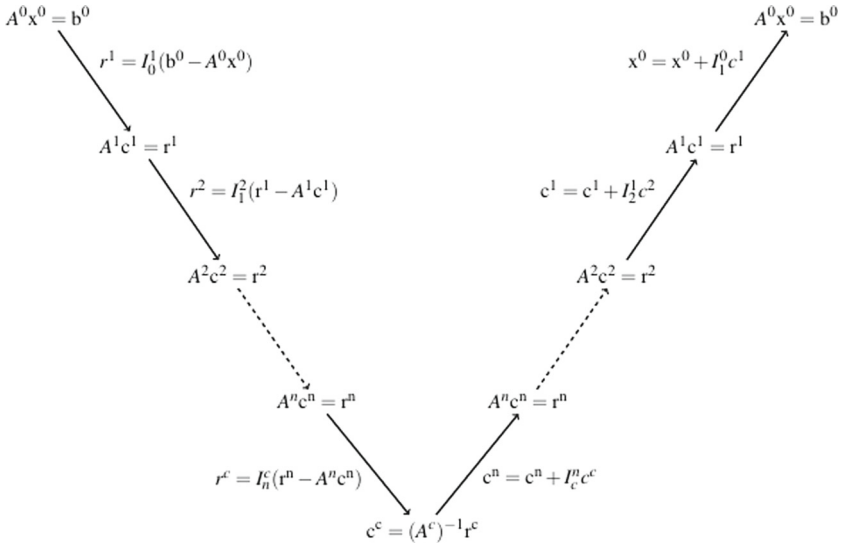

Fig. 1 Schematic of the multigrid V-cycle in the AMG solver

is applied in every iteration as preconditioner to improve the convergence of the solver. For symmetric positive definite systems such as the steady-state groundwater flow equation, the conjugate gradient method is commonly used with MG as preconditioning operator for the residual.

Multigrid methods are not simple to implement while their algorithmic complexity increases significantly in parallel implementation. A few libraries exist, mostly written in C/C++, that offer an object-oriented interface, where users do not deal with many of the algorithmic implementation issues. In this paper, we used two well-known libraries, HYPRE [25] and Trilinos [40]. Both libraries provide interfaces to a variety of numerical tools. In this paper, we apply the multilevel preconditioning package [30] of Trilinos and the BoomerAMG solver [38] provided by HYPRE.

Unlike Krylov subspace methods, MG have many parameters to adjust to achieve optimal performance such as the aggregation method, number of grid levels, type of smoother, type of coarse solver (few smoothing steps may also be used instead of direct solve), and the number of smoothing sweeps. In addition, each of these steps, e.g., each smoother and aggregation, has its own parameter set to configure, e.g., dumping factor, number of sweeps, etc. Overall, the configuration of a multigrid remains a complex task. Although there are default parameter sets for certain problems, proper configuration of AMG methods can increase the efficiency.

The next section provides an outline of a parallel implementation of the NPSAT problem, the application of which is used for a sensitivity analysis of AMG parameters with respect to solving the groundwater flow problem.

4 Parallel implementation of NPSAT

Generally, the construction phase of NPSAT is time-consuming and involves several sequential steps (Fig. 2). However, the memory requirements are relatively small even for large problems and more importantly, the individual processes are embarrassingly parallel, i.e., little or no effort is required to separate the problem into separate tasks and almost no communication between tasks is needed.

The first step in numerical simulation is the discretization of the domain. Because of the complexity of parallel mesh generation and the lack of readily available libraries, in our framework, we choose to construct a 2D mesh using standard methods which can be executed on a single processor. For parallel processing, the 2D mesh is subsequently split into subdomains and the mesh is extruded in the Z direction on each process individually. To allow independent assembly on each processor without the need to exchange information besides the locally owned elements, each subdomain owns a number of ghost elements, which are elements locally owned by another processor. The next step is the matrix assembly where the conductance terms and source/receptor vectors are assembled. The distributed system is solved by the AMG method. Initially, the grids and the restriction and interpolation operators on each level are constructed. The system is then solved iteratively using an appropriate Krylov subspace method with the AMG as preconditioner. In cases where the partial differential equations are non-linear (e.g., unconfined flow), an additional loop is needed which iterates through all steps of the flow problem until the non-linear problem converges. In unconfined groundwater flow simulations, for each non-linear iteration, the elevation of the top layer of the grid becomes equal with the hydraulic head of the previous iteration. This results in a change of the entire conductance

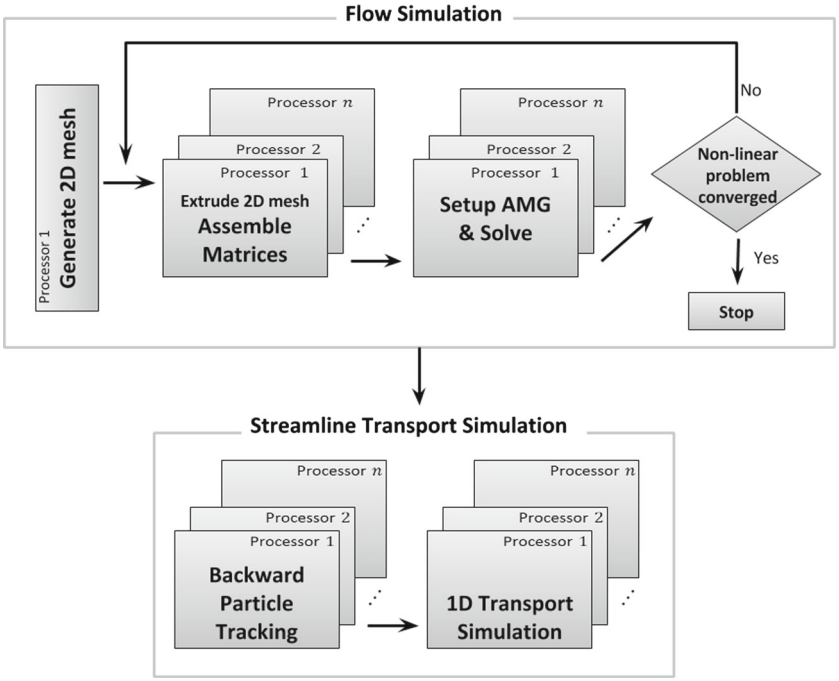

Fig. 2 Flow chart of parallel implementation of the NPS Assessment Tool (NPSAT)

matrix and source/receptors vector. Therefore, the system is reassembled and solved iteratively until the change in the head between two consecutive iterations is smaller than a specified threshold.

The computed head distribution is subsequently used for particle tracking. The streamline tracking simulation is an embarrassingly parallel process. However, it is possible that a single streamline may span multiple subdomains and, hence, multiple processors. In cases where the available memory is able to support the entire 3D mesh, it is advantageous to join the subdomains as streamline tracking becomes easy to implement. When the problem is too large to be stored on a single processor, additional algorithmic effort is needed to transfer particles between processors [67]. The solution of the 1D transport problem along each streamline is an independent process even on very large problems and therefore can easily be parallelized. The implementation phase, which involves convolution of loading functions with the URF computed at the transport simulation, can be parallelized seamlessly although even the serial execution time is typically very small despite a very large number of CDS.

5 Application

5.1 Simulation setup

We apply the parallel implementation of NPSAT to a study area located in the northeastern San Joaquin Valley, California. A coarse steady-state model has been developed by [68] who simulated groundwater flow based on the finite difference method (MODFLOW) using a uniform grid with 400-m cell size and 16 layers for the vertical discretization. The location of the model area is shown in Fig. 3 (thick red line). For our application, necessary input data such as hydraulic conductivity, stresses, boundary conditions, etc. are based on the model of [68]. However, individual well locations are considered vertical lines (points in horizontal cross sections) rather than 400 m × 400 m cell blocks, which yielded a highly resolved finite element version of the Modesto aquifer. The aquifer is approximately 2,600 km^2. The eastern and bottom boundaries are set to have no flow while the top boundary is subject to specified recharge fluxes (Neumann type). General head boundary conditions (Cauchy type) are assigned to the north, south, and west boundaries (Fig. 3). In addition, general head boundary conditions are assigned to the western part of three rivers traversing the modeling domain (Fig. 3, green river segments). The hydraulic conductivity was estimated based on sediment texture analysis and the values span from 0 to 80 m/day (see details in [68]). There is also a confining unit known as Corcoran Clay layer that extends eastward from the western boundary of the aquifer across approximately half of the aquifer (see the red layer in Fig. 4).

The aquifer was discretized using linear prism elements. The element size in the horizontal plane varies between 20 m near wells and rivers and a maximum element length of 300 m. The aquifer contains 1,501 wells distributed across most of the flow domain. This resulted in a very fine unstructured grid with only few areas (e.g., the eastern portions of the aquifer) where finite element size actually

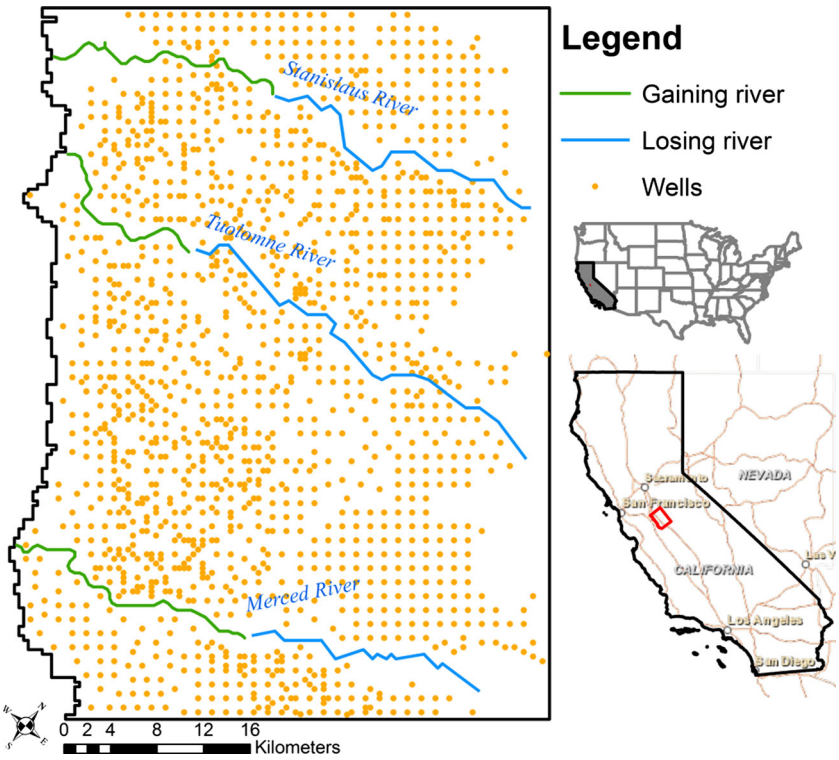

Fig. 3 Location of the Modesto study area in the Central Valley of California. The *red box* corresponds the boundary of the aquifer simulation domain. *Orange dots* identify 1501 pumping wells distributed across the study area

reaches the maximum length size. Vertically, the aquifer was divided into 32 layers, non-uniformly distributed, by increasing the vertical discretization from few meters near the top to several tens of meters toward the bottom. This discretization scheme resulted in a model of 11,514,688 degrees of freedom and approximately 20 million elements.

The NPSAT method first discretizes the domain on a single processor into a 2D triangular mesh consisting of 359,834 nodes using the Gmsh mesh generator package [32]. Next, the 2D mesh was divided into a number of subdomains using the Metis mesh partitioning library [49]. This method attempts to divide the domain into subdomains with equal number of unknowns per subdomain.

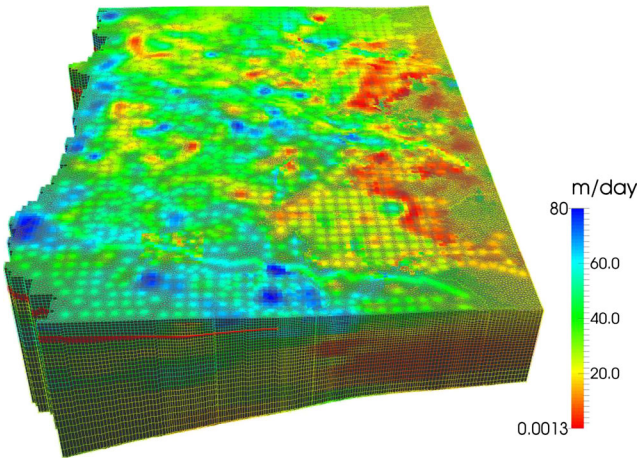

Fig. 4 Hydraulic conductivity field and discretization of the aquifer. Aquifer properties, stresses, and boundary condition data were obtained from Phillips et al. [68]

5.2 AMG comparison and configuration

For the sensitivity analysis of the AMG method, we split the domain into 8, 16, 32, and 64 subdomains, while we assign one processor per subdomain during the solution of linear system with AMG. After the domain partitioning, each processor owns a portion of the 2D triangular mesh. Each processor extrudes its 2D mesh and assembles the system matrix and vectors. The average assembly time per processor is shown in Fig. 5. All runs were executed on a Linux cluster with 2.4 GHz processors and 8 GB RAM per core. For the matrix assembly, we used the NPSAT-based parallel mSim toolbox [52], which solves the groundwater flow equation using continuous Galerkin finite element method. The use of ghost elements circumvents the need for communication between processors during the assembly. Hence, assembly time decreases linearly as the number of processors increases (Fig. 5 red line).

We employed the multilevel preconditioning package (MLPP) by Trilinos (version 11.0.2) and compared it with the BoomerAMG by HYPRE (version 2.9.0). MLPP offers five default AMG configurations targeting different types of

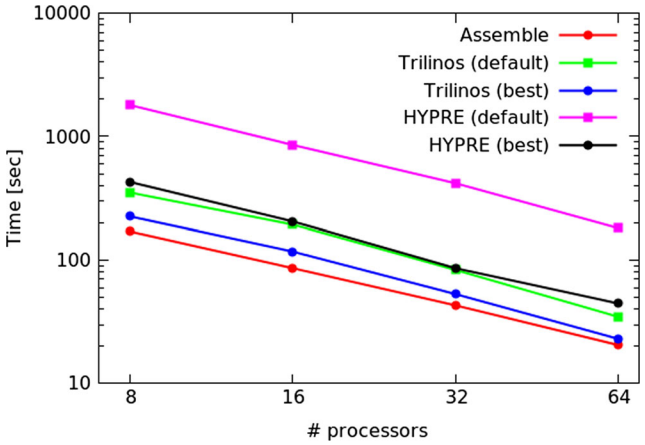

Fig. 5 Comparison of the execution time with various Trilinos and HYPRE Algebraic multigrid configurations for different number of parallel processors

systems of equations. For symmetric positive definite systems, the most suitable configuration is the smooth aggregation (SA) configuration. The SA configuration uses a V-cycle with Gauss–Seidel smoother for all levels, the KLU direct solver [22] for the coarsest level, and an uncoupled followed by a maximal independent set (MIS) technique [77] for the coarsening scheme. Using the default configuration, we solved the 11 million dofs system on eight processors in approximately 6 min. Solver execution time scales linearly with the number of processors resulting in a solution time of about 30 s when 64 processors are used (Fig. 5).

We tested all available smoothers provided by the Trilinos package. Trilinos provides the possibility to also use external solvers as smoothers such as MUMPS [5], UMFPACK [21], or SuperLU [81] which were not tested here. We found that the Chebyshev polynomial smoother [1] significantly improves solver execution time—about twice as fast as in the default configuration. The Chebyshev smoother in MLPP requires two parameters: a polynomial degree and an alpha parameter. We found that the MLPP default values 2 and 20, respectively, gave the minimum solution times. In addition, we examined a number of other parameters and configurations such as the number of sweeps, the number of levels, the type of smoother on the coarsest level, the aggregation method, and the cycle type (i.e., W and F). We found no additional improvements when changing any of those parameters.

When using HYPRE, the default approach is a V-cycle with Falgout coarsening scheme [38] and a hybrid variant of the Gauss–Seidel method. The default HYPRE configuration scales linearly with the number of processors; however, the execution time is approximately 5 times slower compared to the execution time of the default MLPP SA configuration. HYPRE provides 13 types of smoothers (see [44], Section 1 relaxation schemes) and 11 coarsening methods ([44], Section 4). Using 32 processors, we test the efficiency of each method, while keeping the remaining default parameters intact (Fig. 6). Note that some of the methods

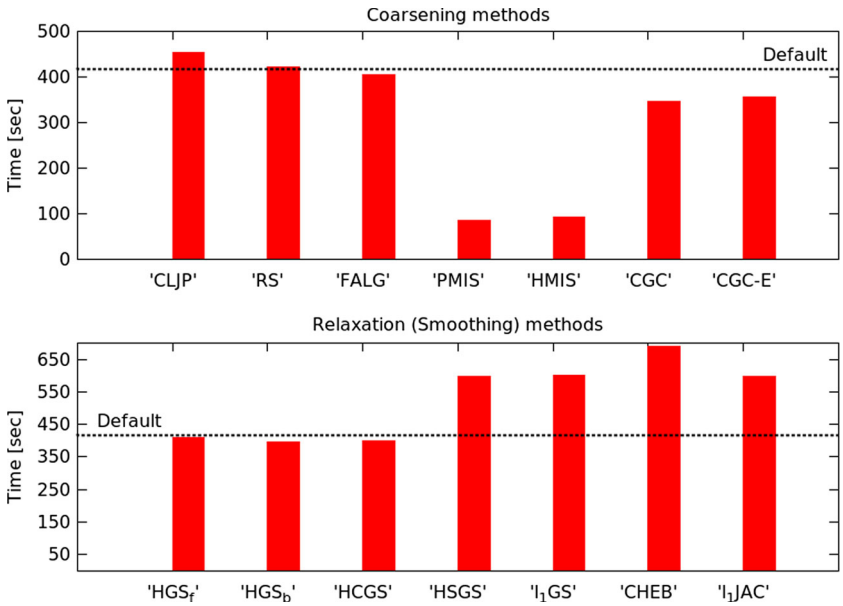

Fig. 6 Efficiency of the coarsening and relaxation methods of HYPRE based on 32 processors. The description of coarsening methods can be found in Griebel et al. [35]. (CLJP: ClearyLubyJonesPlassman, RS: RugeStben,FALG: Falgout, PMIS:Parallel maximal independent set, HMIS: hybrid MIS, CGC:Coarse Grid Classification, CGC-E: CGC with empty coarse grid). The description of relaxation methods is given in HYPRE 2008 (HGSf: Hybrid Gauss-Seidel with forward solve, HGSb: hybrid Gauss-Seidel with backward solve, HCGS: hybrid chaotic Gauss-Seidel, GS: scaled hybrid symmetric Gauss-Seidel, CHEB: Chebyshev, JAC: -scaled Jacobi)

exist for debugging purposes only and those were not tested. Coarsening methods based on variants of the MIS methods significantly improve performance, while other methods are not useful for our application. Relaxation (smoothing) methods based on Gauss–Seidel, the default option, compared favorably in execution time. Interestingly, the Chebyshev smoother, which provided significant improvement in Trilinos, does not appear to reduce the execution time in HYPRE. Varying other parameters in HYPRE, such as type of cycle, number of sweeps, and number of levels, did not further improve execution times.

Both solvers scale linearly with the number of processors. In this particular application, Trilinos appears more efficient compared to HYPRE. Besides the computational efficiency, we note that both libraries require very little programing effort, with 10–20 lines of C++ code sufficient for the AMG implementation.

5.3 NPSAT construction phase

The upper portion of the Modesto subbasin, like most of the Central Valley aquifer, is unconfined. To accurately simulate the water table solution for the unconfined aquifer, we used an outer iteration scheme, for each of which we solve the 11.5 million dof flow problems. At each iteration step, the mesh is deformed according to the previous iteration's head elevation in the top layer. Iterations continue until changes in mesh deformation become insignificant. With mean deformation 5 cm as the convergence criterion for this outer iteration loop, the non-linear water table problem converged after 10 iterations.

The flow simulation results in a highly detailed distribution of the water table surface and of the 3D head potential distribution within the simulation domain (Fig. 7). The water table surface clearly identifies the complex and sharp recharge surface near the meandering streams as they flow from the eastern edge of the groundwater basin toward the San Joaquin River on the western edge of the simulation domain. Approximately halfway across the subbasin and toward the western boundary of the simulation domain, streams submerge below the regional water table and create a relatively sharp, complexly shaped incision within the regional water table, receiving groundwater discharge. Large regional cones of depression within the water table surface (and aquifer) are created through subregional differences in the allocation of surface water to service irrigation and municipal water needs, which yields subregionally varying groundwater pumping stresses. The fine-structured variations in the water table surface (Fig. 7) demonstrate the more localized effects of individual groundwater pumping at varying rates and within varying aquifer materials.

For the streamline transport simulation, we distribute 100 particles around each well screen (four particles at each of

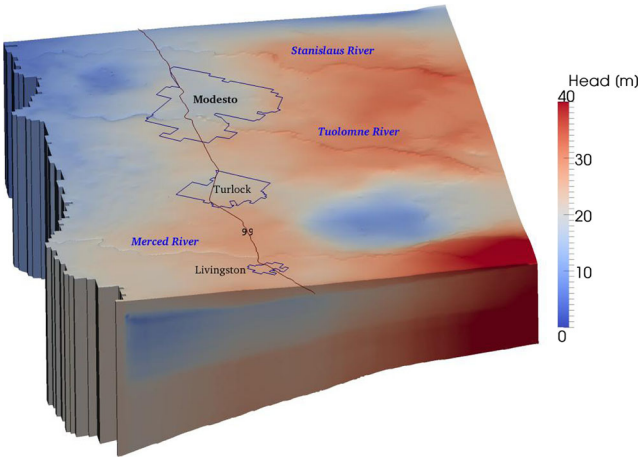

Fig. 7 Shaded three-dimensional representation of the hydraulic head field of the Modesto sub-basin of the Central Valley aquifer. Streams emanate from the Sierra Nevada mountain block in the east (*right side*) and flow towards the San Joaquin River on the western edge (*left side*) of the simulation domain. Streams appear as ridges in the eastern and central portion of the simulation domain, indicating losing conditions (recharge to groundwater). They appear as incised valleys within the water table surface near the San Joaquin River in the western area of the sub-basin, where groundwater is discharging back to the streams. A large cone of depression (appearing as a *blue-colored crater*) is located in the southeastern portion of the sub-basin, where irrigation water is predominantly from wells and surface water rights limit diversions from streams

25 layers). Using backward particle tracking, we compute 150,100 streamlines with their distributed groundwater age (Fig. 8). For the computation, we used the Runge–Kutta–Fehlberg method with adaptive step [52]. The velocity field is computed on the fly during particle tracking for each element based on the head gradient. Figure 8 is a top view of the aquifer; therefore, most of the streamlines depicted there correspond to relatively short, young (near surface) streamlines. Histograms of the age of groundwater entering a well, the depth of the streamline below the water table at the CDS, and the streamline length are shown in Fig. 9. The depth of a streamline below the water table, at its exit point into a CDS, is normally distributed. Yet, the distribution of groundwater age and streamline length are lognormally distributed with relatively long and flat right tails.

At any given time, groundwater of a wide range of age, and of potentially highly varying water quality, enters each well. In large production or agricultural wells with relatively long screen lengths (see Fig. 8 right), the age of the youngest water, entering a well near the top of the screen, varies from 1 to 10 years old. In contrast, depending on the screen length, the age of groundwater entering near the bottom of a production well screen can vary between 100 and more than 1,000 years old.

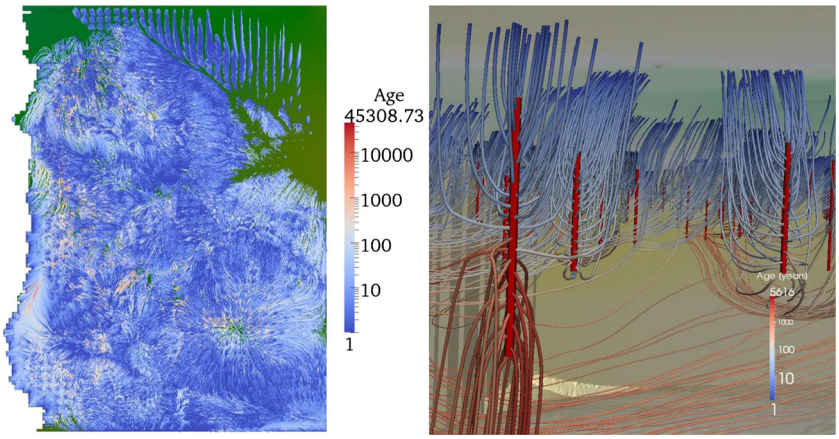

Fig. 8 Three-dimensional spatial distribution of groundwater age along streamlines delivering groundwater to wells (groundwater discharged to streams not shown here). *Dark blue* represents very young water (less than a decade), *intermediate blue* represents water recharged within the last few decades, *light blue* represents water recharged nearly a century ago or longer. *Pink* and *red* colors represent water recharged during pre-Columbian times. Uncertainty about exact water age increases with age due to the focus of the steady state model on average modern-day hydrologic conditions. *Left*: Top view of simulated streamlines showing predominantly the uppermost, shortest and therefore predominantly younger - streamlines. The southeastern area with the cone of depression in the water table (Fig. 7) here shows as an area attracting many of the surrounding streamlines toward the center of the cone. *Right*: Example of the three-dimensional distribution of groundwater ages along streamlines delivering groundwater to production wells (well screens represented as red vertical tubes; not all modeled wells in the view area are shown). The surface at the top represents the water table surface, the surface at the bottom represents the bottom of the aquifer system. Older water enters deeper along the well screen. Younger water is recharged near the well, older water may have been recharged a large distance away and/or may have been upwelling from the depth of the aquifer

The measured pollutant concentration is a flux-weighted average of the concentrations measured along the well screen. To prepare for computing such concentrations, the last step in the construction phase is the computation of unit response functions. Each streamline is discretized into 5-m linear line elements with varying velocity interpolated from the head field via particle tracking. The effective longitudinal dispersivity was set equal to 1/10 of the streamline length to account for aquifer heterogeneity [63]. For the simulation of 1D advection dispersion equation, we used the MATLAB/Octave solvers as the size of each 1D transport problem is small, from 200 to 4,000 degrees of freedom. Similar to the streamline computation, the computation of the URFs for each streamline is executed in parallel.

The transport model can also be used for the simulation of groundwater pollutant contribution to rivers. In our example, three gaining river segments receive groundwater that partly originates from diffuse pollution areas. To identify their source areas, we distribute 13,136 particles around the gaining stream segments (four particles every 20 m, Fig. 10). The majority of streamlines to rivers are less than 3-km long, significantly shorter than streamlines to wells, indicating that rivers receive relatively young water from nearby sources. The water age in discharge to rivers is lognormally distributed with a mean age of 9 years and a maximum age of 170 years. The large difference between river and well streamlines is due to diffuse recharge in the vicinity of a river being the largest contributor to baseflow (groundwater discharge to rivers). It is therefore expected that water quality in discharge into rivers responds to non-point source pollution in the source area similar to shallow

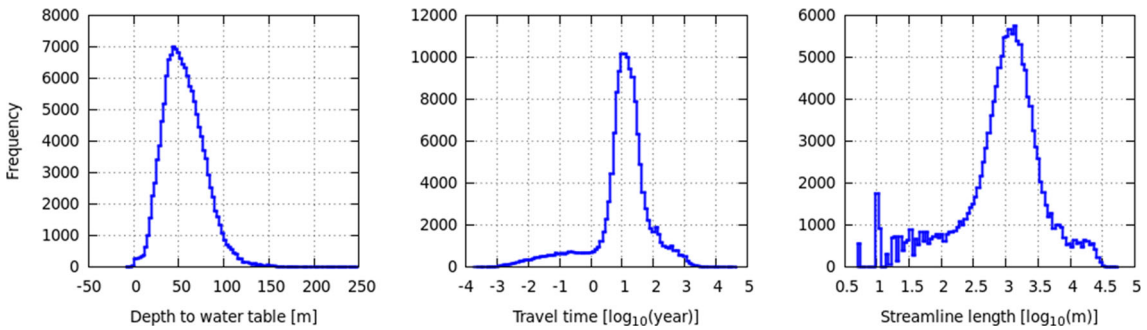

Fig. 9 Histogram of various streamline characteristics; (*left*) depth to water table where the streamline intersects with a well (CDS); (*center*) travel time to the CDS; (*right*) streamline length from source to CDS

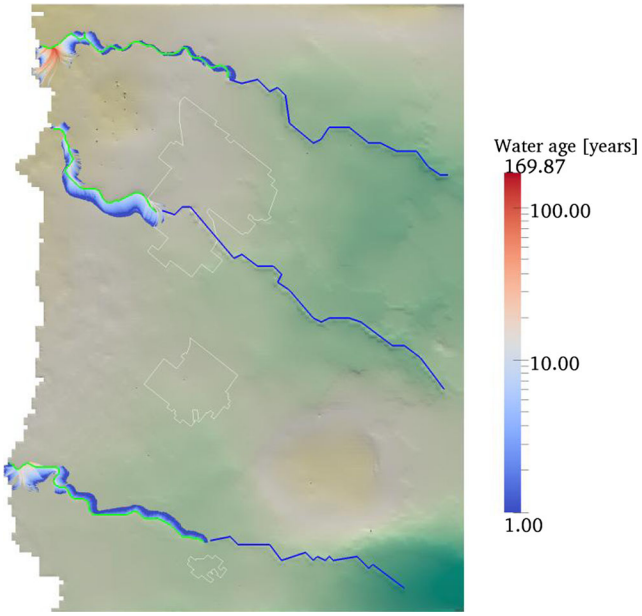

Fig. 10 Groundwater age along streamlines originating from streams. The *green* and *blue* stream segments correspond to gaining and losing streams respectively. *Green-grey* color shading across the study area represents water table height

domestic wells, which also receive relatively younger groundwater.

5.4 Prediction phase

Nitrate transport to groundwater receptors is computed by convoluting nitrate loading functions with the URFs. This second step can be repeated at low computational cost and independent of the construction phase for multiple loading scenarios. These may include actual, projected, hypothetical, or stochastic scenarios, or those defined by various decision-makers, and may or may not account for vadose zone travel times. Here, we choose a representative spatially uniform loading function suggested by [34]. From a set of 200 hydraulic conductivity realizations of the Modesto aquifer, they choose six representative realizations to calibrate the transport parameters, which resulted in six representative nitrate input loading functions to the water table (Fig. 11). In this paper, we extended their 1900–2005 transient loading function by assuming a constant reduction of nitrate loading to about 50% of current loading by the year 2100.

The 150,100 URFs were convolved with the loading function, then integrated via a flux-weighted mean computation to obtain the breakthrough curves for each of the 1,501 wells (thin light gray lines in Fig. 12). Based on the individual breakthrough curves, we computed the percentiles (thick gray lines) across all wells in the subbasin. About 10–20 % of the simulated wells are relatively shallow and closely follow the pattern of the loading function (black dashed line) with a time lag that varies between 5 and 10 years. On the other hand, about 10 % of the deepest wells respond very slowly to the loading function with time lags between 20 and 50 years, where the response is dominated by changes in concentration in the shallow-most water intersected by these wells. Changes in the concentration in deeper sections of these wells occur so slowly that they do not significantly contribute to the dynamics of the breakthrough curve other than significantly dampening the impact of the recent increase in nitrate loading.

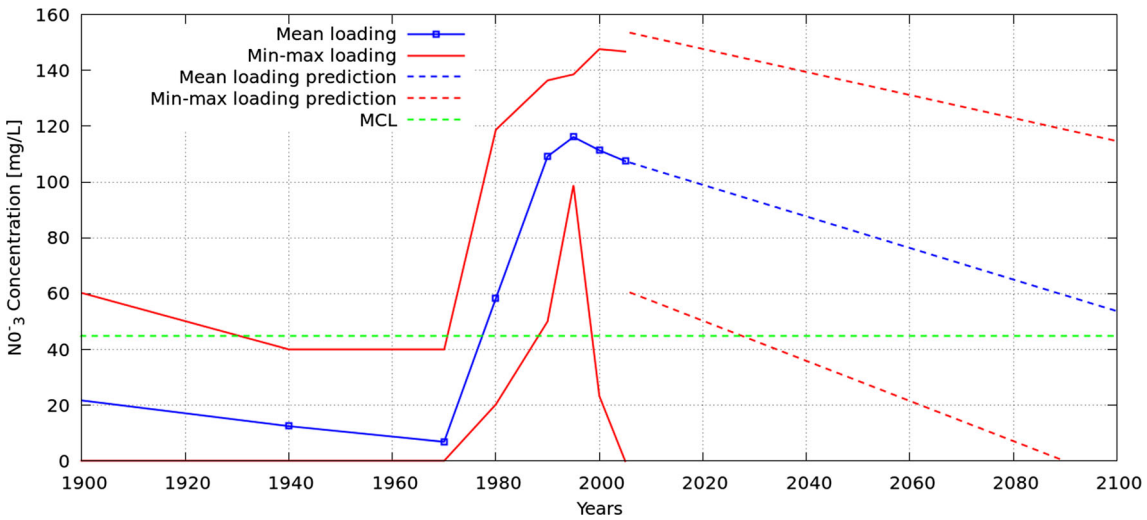

Fig. 11 Representative loading function of nitrate NO_3 to the water table in the Modesto study area. Loading functions are given as probability distribution functions, here showing the minimum, mean, and maximum, varying over time. The *solid lines* are derived from Green et al. [34]. The *dashed lines* correspond to a hypothetical future scenario with continually reduced nitrate loading throughout the 21st century

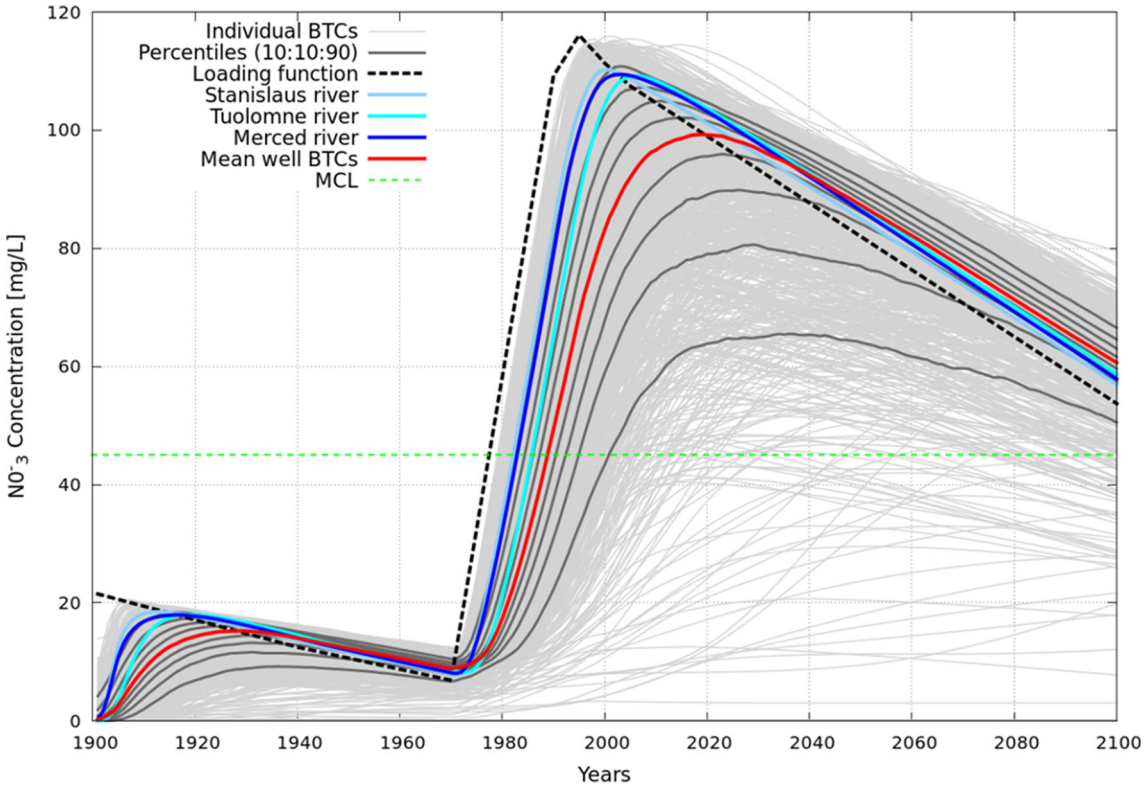

Fig. 12 Nitrate NO_3 breakthrough curves (BTCs) in 1,501 wells (*thin grey*), mean breakthrough (*red*), and percentile concentration distribution (*thick grey*), in steps of (10%) across all wells and gaining rivers (*bluish lines*) in the Modesto sub basin, predicted by the hypothetical loading function (mean loading shown in *black dashed line*). Highest concentrations of nitrate are measured in wells with fast response times, typically shallower wells with relatively short screens

The average BTC (across all production wells) closely follows the loading function, but with several decades delay. The abrupt reduction of loading that occurs in the mid-1990s does not reverse the mean groundwater nitrate until approximately 2025, 30 years later.

In contrast to wells, the river response is significantly faster. The Stanislaus and Merced Rivers respond very similarly with a time lag of approximately 5 years. Only the Tuolomne River has a larger time lag of about 10 years which can be attributed to the fact that groundwater stream lines to the Tuolomne River have a mean length of 1.6 km, significantly longer than the Stanislaus River (0.7 km) and Merced River (0.9 km).

The concept of URFs as a tool for predicting concentration breakthrough curves allows us to run a large number of scenarios using different loading functions with minimal CPU time. This is illustrated here by computing confidence limits to our predictions obtained with the mean loading function. We generate 200 random, first-order auto correlated time-series realizations of spatially uniform, temporally varying nitrate loading functions:

$$L(t) = L(t-1)\varphi + N(\mu(t), \sigma(t))(1-\varphi) \quad (3)$$

where φ expresses the correlation between the years. Here, we choose $\varphi = 0.7$. $\mu(t)$ and $\sigma(t)$ are the transient mean and standard deviation at annual time step t. We assume that loading is normally distributed. We compute a transient standard deviation from the temporally varying reported minimum and maximum values (Fig. 11), $\sigma = \sqrt{n}\left(\mathrm{CI}^{+} - \mathrm{CI}^{-}\right)/\alpha$, where $n = 6$ is the number of samples, CI^{+} and CI^{-} are the upper and lower limits of the confidence intervals, and α is the normalized confidence interval [42]. Due to the small number of samples, the confidence interval α is calculated from the t distribution with upper and lower limits equal to 0.99.

The 200 realizations were convolved with the well URFs to generate 200 BTCs for each well (Fig. 13). The time to convolute 100 URFs with the loading functions, i.e., to compute one well BTC is 6 ms, and the time to compute 1,501 well BTCs is on the order of 9 s; therefore, the time for the stochastic simulation was on the order of 30 min on a serial implementation. When executed in parallel, using a workstation with eight cores, the stochastic simulation time reduces to ~3 min.

The variability at an individual well due to uncertain loading can be quite significant. Figure 13 (right) shows the mean response (solid lines) for five selected wells which

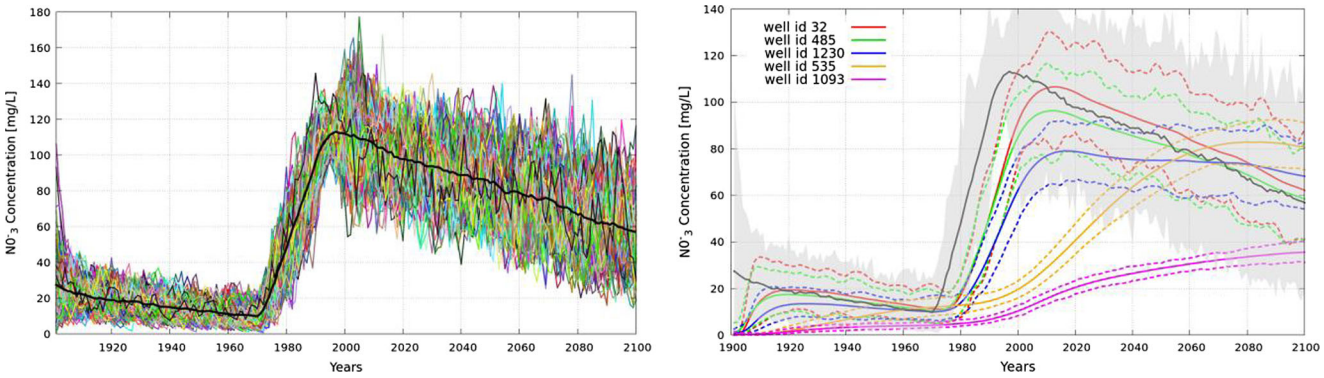

Fig. 13 (*Left*) Stochastic realizations of loading functions. The *black line* correspond to mean loading. (*Right*) Response of five representative wells to stochastic loading scenarios. *Solid lines* represent the mean, *dashed lines* the minimum and maximum values across all realizations

span the entire spectrum of well responses of the Modesto aquifer and the minimum and maximum limits (dashed lines). Shallow wells with short travel times (red, green lines) exhibit greater variability compared to deeper wells associated with large travel times (magenta, orange lines), which can be attributed to the mixing effects that take place in the deep wells. We also see that the yearly temporal variability is smoothed out in the deep wells mainly due to dispersion along the streamlines.

To better understand well response, we group the wells into four categories according to their depth and screen length. Clusters are determined using the k-means method, which attempts to minimize the sums of points-to-cluster-centroid distances (Fig. 14). The first group (green) includes the very shallow wells with depth less than 50 m and screen lengths that vary from a few meters to about 50 m. The screen lengths for the next group of wells (blue) spans from 25 to 75 m and their depths vary between 50 and 90 m. The majority of the screen lengths of the third group spans between 40 and 90 m, yet there are four rather deep wells (about 120 m) with relatively short screen lengths of about 30 m. The well depth for the third group spans from 70 m to 130 m. The last group contains very deep wells with more than 100 m depth and screen lengths greater than 80 m.

For each group of wells, we calculate the median BTC concentration in a given year. For comparison, we also compute a median group BTC obtained by applying the annual mean of the loading realizations to the URFs (Fig. 14 (right)). The time lags from the shallowest to the deepest group vary from 13, 19, and 26 to 38 years, respectively. The stochasticity of the load forcing has practically no impact on the time lag, i.e., the time lag between realizations is very similar. On the other hand, we observe that the maximum range of mean concentration is on the same order (∼23 mg/L)

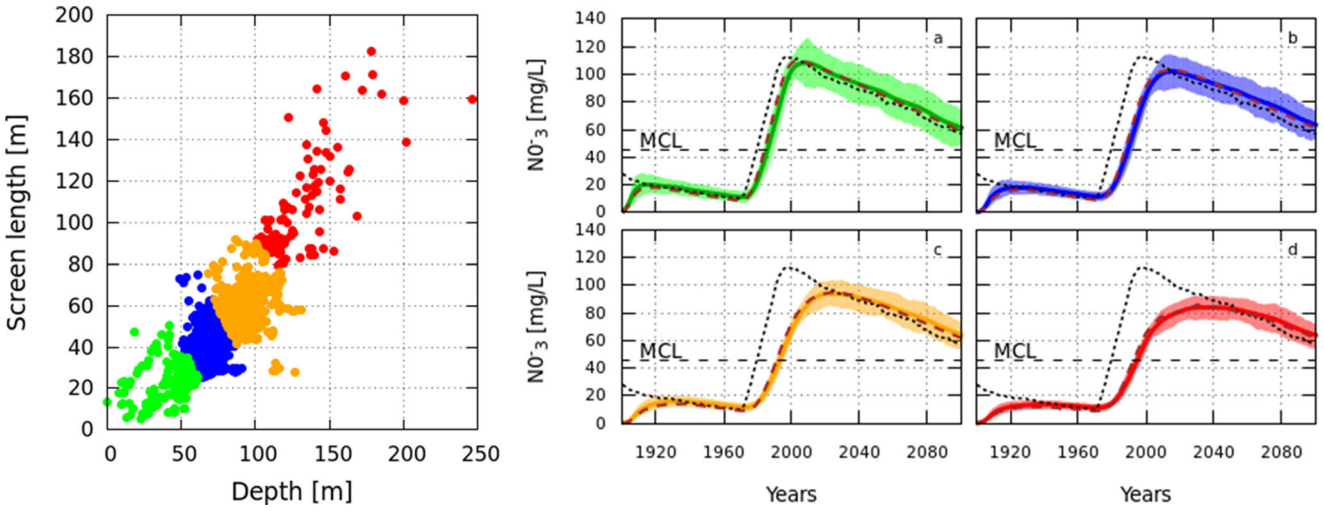

Fig. 14 (*Left*) Well cluster categories based on the screen length and well depth. (*Right*) Mean response of each well group to stochastic forcing. The *solid colored line* corresponds to the mean (from 200 loading realizations) of the median well concentration across 1501 wells. The indicated range is bounded by the annual minimum and maximum median well concentration (from 200 loading realizations). The *dotted line* is the mean stochastic nitrate loading concentration. The *dashed lines* correspond to the median BTC of each group of wells obtained by applying the respective group mean loading function to the URF

for all groups, except the shallowest group which is slightly higher (∼26 mg/L).

By comparing each group's median BTC based on the mean loading function with annual median concentration obtained from the stochastic simulation, we observe that there is very good agreement. But, the stochastic simulation of nitrate loading has the advantage of providing confidence intervals to the estimations, without significantly increasing the computational burden relative to the deterministic simulation.

6 Conclusion

The paper proposes and demonstrates a parallel computational framework for the simulation of non-point source pollution in large groundwater basins, which requires a high-resolution groundwater flow and transport simulation approach. We employed an algebraic multigrid method which was efficiently used as preconditioner to a conjugate gradient method to solve a large groundwater flow problem with ∼11.5 million dofs.

In our study, we compared two AMG implementations, namely, multilevel preconditioning provided by the Trilinos library and Boomer AMG provided by the HYPRE library. Sensitivity analysis of the solver execution time with respect to solver parameters showed that optimal implementation in each library is achieved by quite different configurations. Optimal configuration of AMG is therefore found not only problem-dependent but also library-dependent. With either libraries, in default configuration, the application problem was solved on a single computer with eight processors. Both libraries are shown to scale linearly with the number of processors. Optimizing appropriate coarsening and smoothing methods reduced execution time by 2–5 times. For the solution of the steady-state groundwater flow equation of our application, changing multigrid cycle types or the number of levels did not result in further reduction of the execution time. Sensitivity analysis over the parameters related to the coarsening and smoothing methods indicates that default values are carefully chosen in both libraries as no further improvement was achieved. In our example, Trilinos appears more efficient compared to HYPRE. From implementation point of view, both libraries provide a relatively easy-to-use interface.

We couple the high-resolution groundwater flow solution (less than 20 m near flow receptors and sources) of a 2,600-km^2 groundwater basin to a parallel version of a streamline transport simulator and compute 150,100 URFs to simulate pollutant transport to 1,501 wells and 13,136 URFs to simulate non-point source pollutant transport via groundwater to nearly 65 km of gaining stream segments. The URFs were convolved with a loading function derived from field estimates [34] to simulate 200 years of nitrate transport, from 1900 to 2100. We demonstrate that there is a significant time lag between the time of nitrate loading and response in groundwater wells. The mean aquifer response time varies between 5 and 50 years depending on well depth and screen length. In contrast, the gaining stream segments of the study area respond more rapidly with average time lags of 5 to 10 years.

The efficiency of the URF-based transport simulator lends itself for stochastic simulations of nitrate loading. Here, stochastic transport of nitrate is demonstrated via Monte Carlo simulation of 200 realizations of spatiotemporally distributed nitrate loading across the entire 2,600-km^2 groundwater basin. Two hundred realizations of two centuries of nitrate breakthrough across the 1,501 basin wells are obtained with a total CPU time on the order of 3 min on a standard desktop PC. The BTCs based on mean nitrate loading are similar to the median of BTCs obtained from the stochastic simulation, indicating the usefulness of the mean nitrate loading approach. However, the Monte Carlo simulation also provides a statistical concentration distribution to quantify uncertainty about well (or stream) pollution as a function of time and (arbitrary) geographic subregion.

While the present paper utilizes spatially uniform loading functions for demonstration purposes, the extension to spatially variable loading function due to land-use heterogeneity does not pose an added computational burden. Future work will evaluate the impact of spatial heterogeneity in nitrate loading. Importantly, with these short CPU times, the transport simulation tool can be employed for agronomic systems optimization, as a planning tool, or as part of Bayesian statistical or other Monte Carlo simulation-based inverse modeling approaches.

Acknowledgments The authors wish to thank the two anonymous reviewers for their constructive comments. This work was supported by the California State Water Resources Control Board under agreement number 09-122-250 and by the California Department of Food and Agriculture under agreement number FREP 11-0301.

References

1. Adams, M., Brezina, M., Hu, J., Tuminaro, R.: Parallel multigrid smoothing: polynomial versus Gauss-Seidel. J. Comput. Phys. **188**(2), 593–610 (2003). doi:10.1016/S0021-9991(03)00194-3
2. Aller, L., Bennett, T., Lehr, J.H., Petty, R.J., Hackett, G.: DRASTIC: a standardized system for evaluating groundwater pollution potential using hydrogeologic settings, Rep. EPA-600/2-87-035, pp. 641, U.S. Environ. Prot. Agency, Ada, Okla (1987)
3. Al-Mahallawi, K., Mania, J., Hani, A., Shahrour, I.: Using of neural networks for the prediction of nitrate groundwater contamination in rural and agricultural areas. Environ. Earth. Sci. **65**, 917–928 (2012). doi:10.1007/s12665-011-1134-5

4. Almasri, M.N., Kaluarachchi, J.: Modeling nitrate contamination of groundwater in agricultural watersheds. J. Hydrol. **343**, 211–229 (2007)
5. Amestoy, P.R., Duff, I.S., l'Excellent, J.-Y.: Multifrontal parallel distributed symmetric and unsymmetric solvers. Comput. Methods Appl. Mech. Eng. **184**(2–4), 501–520 (2000). doi:10.1016/S0045-7825(99)00242-X
6. Ashby, S.F., Falgout, R.D.: A parallel multigrid preconditioned conjugate gradient algorithm for groundwater flow simulations. Nucl. Sci. Eng. **124**, 145–159 (1996)
7. Bandilla, K.W., Rabideau, A.J., Jankovic, I.: A parallel mesh-free contaminant transport model based on the Analytic Element and Streamline Methods. Adv. Water Resour. **32**, 1143–1153 (2009)
8. Batycky, R.P., Blunt, M.J., Thiele, M.R.: A 3D field-scale streamline-based reservoir simulator. SPE Reserv. Eng. **12**(4), 246–254 (1997)
9. Benali, A.: Groundwater modelling: towards an estimation of the acceleration factors of iterative methods via an analysis of the transmissivity spatial variability. Compt. Rendus Geosci. **345**(1), 36–46 (2013)
10. Beraldo, V.T., Blunt, M.J., Schiozer, D.J.: Compressible streamline-based simulation with changes in oil composition. SPE Reserv. Eval. Eng. **12**(6), 963–973 (2009)
11. Bernardo, D.J., Mapp, H.P., Sabagh, G.J., Geleta, S., Watkins, K.B., Elliott, R.L., Stone, J.F.: Economic and environmental impacts of water quality protection policies 2. Application to the Central High Plains. Water Resour. Res. **29**(9), 3081–3091 (1993)
12. Blunt, M.J., Liu, K., Thiele, M.R.: A generalized streamline method to predict reservoir flow. Petrol. Geosci. **2**(2), 259–269 (1996). doi:10.1144/petgeo.2.3.259
13. Bonton, A., Bouchard, C., Rouleau, A., Rodriguez, M.J., Therrien, R.: Calibration and validation of an integrated nitrate transport model within a well capture zone. J. Contam. Hydrol. **128**, 1–18 (2012)
14. Bonton, A., Rouleau, A., Bouchard, C., Rodriguez, M.J.: Nitrate transport modeling to evaluate source water protection scenarios for a municipal well in an agricultural area. Agr. Syst. **104**, 429–439 (2011)
15. Brandt, A., Livne, O.E.: Multigrid Techniques: 1984 guide with applications to fluid dynamics Rev. ed. SIAM (2011)
16. Briggs, W.L., Henson, V.E., McCormick, S.F.: A Multigrid Tutorial 2nd Edn, SIAM, pp. 193 (2000)
17. Bundy, B.C., Hales, H.B.: A streamline reservoir simulator with dynamic gridding. J. Can. Petrol. Technol. **47**(2), 32–38 (2008)
18. Burow, K.R., Nolan, B.T., Rupert, M.G., Dubrovsky, N.M.: Nitrate in groundwater of the United States, 1991-2003. Environ. Sci. Technol. **44**, 4988–4997 (2010). doi:10.1021/es100546y
19. Cirpka, O.A., Kitanidis, P.K.: Characterization of mixing and dilution in heterogeneous aquifers by means of local temporal moments. Water Resour. Res. **36**(5), 1221–1236 (2000)
20. Collins, A.L., McGonigle, D.F.: Monitoring and modelling diffuse pollution from agriculture for policy support: UK and European experience. Environ. Sci. Policy **11**(1), 97–101 (2008)
21. Davis, T.A.: Algorithm 832: UMFPACK, an unsymmetric-pattern multifrontal method. ACM Trans. Math. Soft. **30**(1), 196–199 (2004)
22. Davis, T.A., Palamadai Natarajan, E.: Algorithm 907 KLU, A direct sparse solver for circuit simulation problems. ACM Trans. Math. Soft. **37**(2) (2010). doi:10.1145/1824801.1824814. Article 36
23. Elci, A., Karadas, D., Fıstıkoglu, O.: The combined use of MODFLOW and precipitation-runoff modeling to simulate groundwater flow in a diffuse-pollution prone watershed. Water Sci. Technol. **62**(1), 180–188 (2010)
24. Enzenhoefer, R., Bunk, T., Nowak, W.: Nine steps to risk-informed wellhead protection and management: a case study. Ground Water (2014)
25. Falgout, R.D., Yang, U.M.: Hypre: A library of high performance preconditioners in computational science—ICCS 2002 part III. In: Sloot, P.M.A., Tan, C.J.K., Dongarra, J.J., Hoekstra, A.G. (eds.): vol. 2331 of Lecture Notes in Computer Science, pp. 632–641. Springer (2002)
26. Fang, J., Ding, Y.-J.: Assessment of groundwater contamination by NO3 using geographical information system in the Zhangye Basin, Northwest China. Environ. Earth Sci. **60**, 809–816 (2010). doi:10.1007/s12665-009-0218-y
27. Flipo, N., Jeannee, N., Poulin, M., Even, S., Ledoux, E.: Assessment of nitrate pollution in the Grand Morin aquifers (France): combined use of geostatistics and physically based modeling. Environ. Pollut. **146**(1), 241–256 (2007). doi:10.1016/j.envpol.2006.03.056
28. Galbiati, L., Bouraoui, F., Elorza, F.J., Bidoglio, G.: Modeling diffuse pollution loading into a Mediterranean lagoon: development and application of an integrated surface-subsurface model tool. Ecol. Model **193**, 4–18 (2006)
29. Gallardo, A.H., Reyes-Borja, W., Tase, N.: Flow and patterns of nitrate pollution in groundwater: a case study of an agricultural area in Tsukuba City, Japan. Environ. Geol. **48**, 908–919 (2005). doi:10.1007/s00254-005-0029-8
30. Gee, M.W., Siefert, C.M., Hu, J.J., Tuminaro, R.S., Sala, M.G.: ML 5.0 Smoothed Aggregation User's Guide, Sandia National Laboratories, SAND2006-2649 (2006)
31. Gelhar, L.W., Welty, C., Rehfeldt, K.R.: A critical review of data on field-scale dispersion in aquifers. Water Resour. Res. **28**(7), 1955–1974 (1992). doi:10.1029/92WR00607
32. Geuzaine, C., Remacle, J.F.: Gmsh: A three-dimensional finite element mesh generator with built-in pre- and post-processing facilities. Int. J. Numer. Methods Eng. **79**(11), 1309–1331 (2009)
33. Ginn, T.: Stochastic–convective transport with nonlinear reactions and mixing: finite streamtube ensemble formulation for multicomponent reaction systems with intra-streamtube dispersion. J. Contam. Hydrol. **47**, 1–8 (2001)
34. Green, C.T., Böhlke, J.K., Bekins, B.A., Phillips, S.P.: Mixing effects on apparent reaction rates and isotope fractionation during denitrification in a heterogeneous aquifer. Water Resour. Res. **46**, W08525 (2010). doi:10.1029/2009WR008903
35. Griebel, M., Metsch, B., Oeltz, D., Schweitzer, M.A.: Coarse grid classification: a parallel coarsening scheme for algebraic multigrid methods. Numer. Linear Algebra Appl. **13**(1), 193–214 (2006). doi:10.1002/nla.482
36. Harter, T., Morel-Seytoux, H.: Peer review of the IWFM, MODFLOW and HGS model codes: potential for water management applications in California's Central Valley and other irrigated groundwater basins. Final Report, California Water and Environmental Modeling Forum, August 2013, Sacramento (2013). http://www.cwemf.org
37. Harter, T., Lund, J.R., Darby, J., Fogg, G.E., Howitt, R., Jessoe, K.K., Pettygrove, G.S., Quinn, J.F., Viers, J.H., Boyle, D.B., Canada, H.E., DeLaMora, N., Dzurella, K.N., Fryjoff-Hung, A., Hollander, A.D., Honeycutt, K.L., Jenkins, M.W., Jensen, V.B., King, A.M., Kourakos, G., Liptzin, D., Lopez, E.M., Mayzelle, M.M., McNally, A., Medellin-Azuara, J., Rosenstock, T.S.: Addressing nitrate in California's drinking water with a focus on Tulare Lake basin and Salinas Valley groundwater. Report for the State Water Resources Control Board Report to the Legislature. Center for Watershed Sciences,University of California, Davis, 78 p. (2012). http://groundwaternitrate.ucdavis.edu

38. Henson, V.E., Yang, U.M.: BoomerAMG: a parallel algebraic multigrid solver and preconditioner. Appl. Numer. Math. **41**, 155–177 (2000)
39. Herrera, P.A., Valocchi, A.J., Beckie, R.D.: A multidimensional streamline-based method to simulate reactive solute transport in heterogeneous porous media. Adv. Water Resour. **33**, 711–727 (2010)
40. Heroux, M., Bartlett, R., Hoekstra, V.H.R., Hu, J., Kolda, T., Lehoucq, R., Long, K., Pawlowski, R., Phipps, E., Salinger, A., Thornquist, H., Tuminaro, R., Willenbring, J., William, A.: An overview of Trilinos, Sandia National Laboratories, SAND2003-2927 (2003)
41. Hewett, C.J.M., Quinn, P.F., Heathwaite, A.L., Doyle, A., Burke, S., Whitehead, P.G., Lerner, D.N.: A multi-scale framework for strategic management of diffuse pollution. Environ. Modell. Softw. **24**, 74–85 (2009)
42. Higgins, J.P.T., Green, S. (eds.): Cochrane Handbook for Systematic Reviews of Interventions Version 5.0.0 [updated February 2008]. The Cochrane Collaboration, 2008. (2008). www.cochrane-handbook.org
43. Howden, N.J.K., Burt, T.P., Worrall, F., Mathias, S., Whelan, M.J.: Nitrate pollution in intensively farmed regions: what are the prospects for sustaining high-quality groundwater?. Water Resour. Res. **47**, W00L02 (2011). doi:10.1029/2011WR010843
44. HYPRE: Reference Manual, Lawrence Livermore National Laboratory (2008). http://computation.llnl.gov/casc/hypre/software.html
45. Jeong, D., Choe, J., Park, K.: Analyses of solute transport using streamline simulation and semianalytical solutions, Energy sources, part A: Recover. Utilization Environ. Eff. **30**(11), 1027–1037 (2008). doi:10.1080/15567030601082399
46. Jiang, Y., Somers, G.: Modeling effects of nitrate from non-point sources on groundwater quality in an agricultural watershed in Prince Edward Island, Canada. Hydrogeol. J. **17**, 707–724 (2009)
47. Joosten, L.T.A., Buijze, S.T., Jansen, D.M.: Nitrate in sources of drinking water? Dutch water companies aim at prevention. Environ. Pollut. **102**(S1), 487–492 (1998)
48. Kaown, D., Hyun, Y., Bae, G.-O., Lee, K.-K.: Factors affecting the spatial pattern of nitrate contamination in shallow groundwater. J. Environ. Qual. **36**, 1479–1487 (2007)
49. Karypis, G.: A Software Package for Partitioning Unstructured Graphs, Partitioning Meshes, and Computing Fill-Reducing Orderings of Sparse Matrices, Version 5.0. University of Minnesota, Minneapolis (2011)
50. Khalil, A., Almasri, M.N., McKee, M., Kaluarachchi, J.J.: Applicability of statistical learning algorithms in groundwater quality modeling. Water Resour. Res. **41**, W05010 (2005). doi:10.1029/2004WR003608
51. Kourakos, G., Klein, F., Cortis, A., Harter, T.: A groundwater nonpoint source pollution modeling framework to evaluate long-term dynamics of pollutant exceedance probabilities in wells and other discharge locations. Water Resour. Res. **48**, W00L13 (2012). doi:10.1029/2011WR010813
52. Kourakos, G., Harter, T.: Vectorized simulation of groundwater flow and streamline transport. Environ. Modell. Soft. **52**, 207–221 (2014). doi:10.1016/j.envsoft.2013.10.029
53. Ledoux, E., Gomez, E., Monget, J.M., Viavattene, C., Viennot, P., Ducharne, A., Benoit, M., Mignolet, C., Schott, C., Mary, B.: Agriculture and groundwater nitrate contamination in the Seine basin. The STICS-MODCOU modelling chain. Sci. Total Environ. **375**, 69–79 (2007). doi:10.1016/j.scitotenv.2006.12.002
54. Liao, L., Green, C.T., Bekins, B.A., Bohlke, J.K.: Factors controlling nitrate fluxes in groundwater in agricultural areas. Water Resour. Res. **48**, W00L09 (2012). doi:10.1029/2011WR011008
55. Liu, X.: Parallel modeling of three-dimensional variably saturated ground water flows with unstructured mesh using open source finite volume platform Openfoam. Eng. Appl. Comput. Fluid Mech. **7**(1), 223–238 (2013)
56. Martin, C., Molenat, J., Gascuel-Odoux, C., Vouillamoz, J.-M., Robain, H., Ruiz, L., Faucheux, M., Aquilina, L.: Modelling the effect of physical and chemical characteristics of shallow aquifers on water and nitrate transport in small agricultural catchments. J. Hydrol. **326**, 25–42 (2006)
57. Martinez, Y., Albiac, J.: Agricultural pollution control under Spanish and European environmental policies. Water Resour. Res. **40**, W10501 (2004). doi:10.1029/2004WR003102
58. McMahon, P.B., Burow, K.R., Kauffman, L.J., Eberts, S.M., Böhlke, J.K., Gurdak, J.J.: Simulated response of water quality in public supply wells to land use change. Water Resour. Res. **44**, W00A06 (2008). doi:10.1029/2007WR006731
59. Molenat, J., Gascuel-Odoux, C.: Modelling flow and nitrate transport in groundwater for the prediction of water travel times and of consequences of land use evolution on water quality. Hydrol. Process. **16**, 479–492 (2002). doi:10.1002/hyp.328
60. Murgulet, D., Tick, G.R.: Assessing the extent and sources of nitrate contamination in the aquifer system of southern Baldwin County, Alabama. Environ. Geol. **58**, 1051–1065 (2009). doi:10.1007/s00254-008-1585-5
61. Mustapha, H., Ghorayeb, A., Mustapha, K.: Complex flow simulation in natural aquifer: an algorithm for parallel flow simulations in the finite element framework. Adv. Eng. Inform. **27**(1), 149–156 (2009)
62. National Research Council: Groundwater vulnerability assessment: Predicting relative contamination potential under conditions of uncertainty, pp. 204. National Academy Press, Washington (1993)
63. Neuman, S.P.: Universal scaling of hydraulic conductivities and dispersivities in geologic media. Water Resour. Res. **26**(8), 1749–1758 (1990). doi:10.1029/WR026i008p01749
64. Nolan, B., Hitt, K.J.: Vulnerability of shallow groundwater and drinking-water wells to nitrate in the United States. Environ. Sci. Technol. **40**(24), 7834–7840 (2006)
65. Nolan, B., Ruddy, B.C., Hitt, K.J., Helsel, D.R.: Risk of Nitrate in groundwaters of the United States a national perspective. Environ. Sci. Technol. **31**, 2229–2236 (1997)
66. Obi, E.-O., Blunt, M.J.: Streamline-based simulation of advective–dispersive solute transport. Adv. Water Resour. **27**, 913–924 (2004)
67. Peterka, T., Ross, R.B., Nouanesengsy, B., Lee T-Y, Shen, H.-W., Kendall, W., Huang, J.: A study of parallel particle tracing for steady-state and time-varying flow fields. In proceeding of: 25th IEEE International Symposium on Parallel and Distributed Processing, IPDPS 2011, Anchorage, Alaska, USA, 16-20 May (2011)
68. Phillips, S.P., Green, C.T., Burow, K.R., Shelton, J.L., Rewis, D.L.: Simulation of multiscale groundwater flow in part of the northeastern San Joaquin Valley, California: U.S. Geol. Surv. Sci. Investig. Rep. **2007–5009**, 43 (2007)
69. Refsgaarda, J.C., Thorsena, M., Jensena, J.B., Kleeschulteb, S., Hansen, S.: Large scale modelling of groundwater contamination from nitrate leaching. J. Hydrol. **221**, 117–140 (1999). doi:10.1016/S0022-1694(99)00081-5
70. Saad, Y.: Iterative methods for sparse linear systems. Society for Industrial and Applied Mathematics, Philadelphia (2003)
71. Snyder, D.T., Wilkinson, J.M., Orzol, L.L.: Use of a ground-water flow model with particle tracking to evaluate ground-water vulnerability, Clark County, Washington. U.S. Geological Survey. USGS Water-Supply Paper 2488, Denver (1998)

72. Spalding, R.F., Exner, M.E.: Occurrence of nitrate in groundwater–a review. J. Environ. Qual. **22**, 32–402 (1993)
73. Starn, J.J., Bagtzoglou, A.C., Robbins, G.A.: Methods for simulating solute breakthrough curves in pumping groundwater wells. Comput. & Geosci. **48**, 244–255 (2012). doi:10.1016/j.cageo.2012.01.011
74. Starn, J.J., Bagtzoglou, A.C., Robbins, G.A.: Uncertainty in simulated groundwater quality trends in transient flow. Hydrogeol. J. **21**(4), 813–827 (2013)
75. Sutton, M.A., Howard, C.M., Erisman, J.W.: The European nitrogen assessment. 664 (2011)
76. Thorburn, P.J., Biggs, J.S., Weier, K.L., Keating, B.A.: Nitrate in groundwaters of intensive agricultural areas in coastal Northeastern Australia. Agr Ecosyst Environ **94**, 49–58 (2003)
77. Tuminaro, R., Tong, C.: Parallel smoothed aggregation multigrid: Aggregation strategies on massively parallel machines in Super Computing 2000 Proceeding Donnelley, J. (ed.) (2000)
78. U.S. EPA.: Integrated Science Assessment for Oxides of Nitrogen—Health Criteria (Final Report). U.S. Environmental Protection Agency, Washington, DC, EPA/600/R-08/071. (2008)
79. Weissmann, G.S., Zhang, Y., LaBolle, E.M., Fogg, G.E.: Dispersion of groundwater age in an alluvial aquifer system. Water Resour. Res. **38**(10), 1198 (2002). doi:10.1029/2001WR000907
80. Wriedt, G., Rode, M.: Modelling nitrate transport and turnover in a lowland catchment system. J. Hydrol. **328**, 157–176 (2006)
81. Xiaoye, S.L.: An overview of SuperLU: Algorithms, implementation, and user interface. TOMS **31**(3), 302–325 (2005)
82. Yesilnacar, M.I., Sahinkaya, E.: Artificial neural network prediction of sulfate and SAR in an unconfined aquifer in southeastern Turkey. Environ. Earth Sci. **67**, 1111–1119 (2012). doi:10.1007/s12665-012-1555-9